



HAL
open science

Chiral Radical Cation Salts of Me-EDT-TTF and DM-EDT-TTF with Octahedral, Linear and Tetrahedral Monoanions

Nabil Mroweh, Alexandra Bogdan, Flavia Pop, Pascale Auban-Senzier, Nicolas Vanthuyne, Elsa B Lopes, Manuel Almeida, Narcis Avarvari

► **To cite this version:**

Nabil Mroweh, Alexandra Bogdan, Flavia Pop, Pascale Auban-Senzier, Nicolas Vanthuyne, et al.. Chiral Radical Cation Salts of Me-EDT-TTF and DM-EDT-TTF with Octahedral, Linear and Tetrahedral Monoanions. *Magnetochemistry*, 2021, 7 (6), pp.87. 10.3390/magnetochemistry7060087 . hal-03452274

HAL Id: hal-03452274

<https://univ-angers.hal.science/hal-03452274v1>

Submitted on 26 Nov 2021

HAL is a multi-disciplinary open access archive for the deposit and dissemination of scientific research documents, whether they are published or not. The documents may come from teaching and research institutions in France or abroad, or from public or private research centers.

L'archive ouverte pluridisciplinaire **HAL**, est destinée au dépôt et à la diffusion de documents scientifiques de niveau recherche, publiés ou non, émanant des établissements d'enseignement et de recherche français ou étrangers, des laboratoires publics ou privés.



Distributed under a Creative Commons Attribution 4.0 International License

Article

Chiral Radical Cation Salts of Me-EDT-TTF and DM-EDT-TTF with Octahedral, Linear and Tetrahedral Monoanions †

Nabil Mroweh ¹, Alexandra Bogdan ¹ , Flavia Pop ¹, Pascale Auban-Senzier ², Nicolas Vanthuyne ³ ,
Elsa B. Lopes ⁴ , Manuel Almeida ⁴  and Narcis Avarvari ^{1,*} 

¹ Univ Angers, CNRS, MOLTECH-Anjou, SFR MATRIX, F-49000 Angers, France; nabil.mroweh@cea.fr (N.M.); alexandra.bogdan@etud.univ-angers.fr (A.B.); flavia.pop@univ-angers.fr (F.P.)

² Laboratoire de Physique des Solides, Université Paris-Saclay CNRS UMR 8502, Bât. 510, 91405 Orsay, France; pascale.senzier@universite-paris-saclay.fr

³ Aix Marseille Université, CNRS, Centrale Marseille, iSm2, 13013 Marseille, France; nicolas.vanthuyne@univ-amu.fr

⁴ Centro de Ciências e Tecnologias Nucleares (C2TN) and Departamento de Engenharia e Ciências Nucleares (DECN), Instituto Superior Técnico (IST), Universidade de Lisboa, E.N. 10, 2695-066 Bobadela LRS, Portugal; eblopes@ctn.tecnico.ulisboa.pt (E.B.L.); malmeida@ctn.tecnico.ulisboa.pt (M.A.)

* Correspondence: narcis.avarvari@univ-angers.fr; Tel.: +33-2-4173-5084

† Dedicated to the memory of Professor Peter Day.

Abstract: Methyl-ethylenedithio-tetrathiafulvalene (Me-EDT-TTF (**1**)) and dimethyl-ethylenedithio-tetrathiafulvalene (DM-EDT-TTF (**2**)) are valuable precursors for chiral molecular conductors, which are generally obtained by electrocrystallization in the presence of various counter-ions. The number of the stereogenic centers, their relative location on the molecule, the nature of the counter-ion and the electrocrystallization conditions play a paramount role in the crystal structures and conducting properties of the resulting materials. Here, we report the preparation and detailed structural characterization of the following series of radical cation salts: (i) mixed valence (1)₂AsF₆ as racemic, and (S) and (R) enantiomers; (ii) [(S)-1]AsF₆·C₄H₈O and [(R)-1]AsF₆·C₄H₈O where a strong dimerization of the donors is observed; (iii) (1)I₃ and (2)I₃ as racemic and enantiopure forms and (iv) [(*meso*)-2]PF₆ and [(*meso*)-2]XO₄ (X = Cl, Re), based on the new donor (*meso*)-2. In the latter, the two methyl substituents necessarily adopt axial and equatorial conformations, thus leading to a completely different packing of the donors when compared to the chiral form (S,S)/(R,R) of **2** in its radical cation salts. Single crystal resistivity measurements, complemented by thermoelectric power measurements in the case of (1)₂AsF₆, suggest quasi-metallic conductivity for the latter in the high temperature regime, with $\sigma_{RT} \approx 1\text{--}10 \text{ S cm}^{-1}$, while semiconducting behavior is observed for the (*meso*)-2 based salts.

Keywords: organic conductors; chirality; tetrathiafulvalene; EDT-TTF; crystal structures; electrical conductivity



Citation: Mroweh, N.; Bogdan, A.; Pop, F.; Auban-Senzier, P.; Vanthuyne, N.; Lopes, E.B.; Almeida, M.; Avarvari, N. Chiral Radical Cation Salts of Me-EDT-TTF and DM-EDT-TTF with Octahedral, Linear and Tetrahedral Monoanions. *Magnetochemistry* **2021**, *7*, 87. <https://doi.org/10.3390/magnetochemistry7060087>

Academic Editor: Fabrice Pointillart

Received: 27 May 2021

Accepted: 16 June 2021

Published: 20 June 2021

Publisher's Note: MDPI stays neutral with regard to jurisdictional claims in published maps and institutional affiliations.

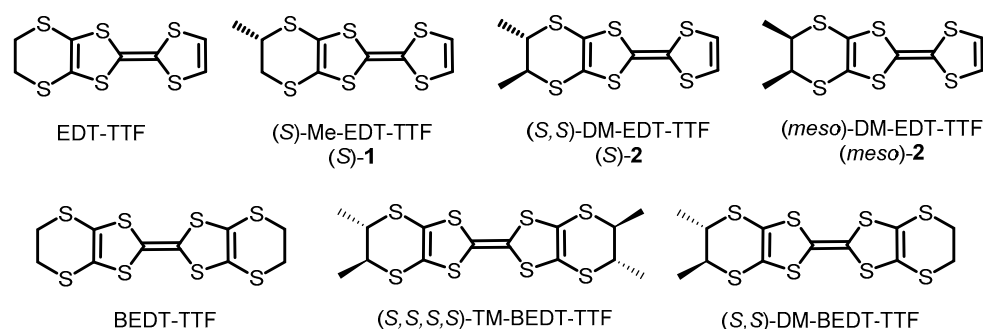


Copyright: © 2021 by the authors. Licensee MDPI, Basel, Switzerland. This article is an open access article distributed under the terms and conditions of the Creative Commons Attribution (CC BY) license (<https://creativecommons.org/licenses/by/4.0/>).

1. Introduction

Substitution of a hydrogen atom at one or both carbon atoms of the ethylene bridge of the ethylenedithio-tetrathiafulvalene (EDT-TTF) precursor generates one or two stereogenic centers, respectively, as in methyl-EDT-TTF (Me-EDT-TTF) **1** and dimethyl-EDT-TTF (DM-EDT-TTF) **2**, thus providing chiral tetrathiafulvalenes [1,2] (Scheme 1). These precursors proved to be highly valuable since they afforded by electrocrystallization a series of enantiopure and racemic radical cation salts showing chirality and anion-dependent crystalline packing and conducting properties. For example, donor **1**, which has been only recently described [3], provided the complete series of mixed-valence salts (1)₂PF₆, with metal-like conductivity [3], while with the perchlorate anion only the enantiopure salts, formulated as [(S)-1]₂ClO₄ and [(R)-1]₂ClO₄, showed metallic conductivity in the high-temperature regime, the racemic form [(*rac*)-1]ClO₄ being a very poor conductor because of the formation of strong heterochiral dimers by the radical cations [4]. On the other hand,

the dimethylated donor **2**, containing two stereogenic centers (*S,S*) or (*R,R*) afforded semi-conducting 4:2 enantiopure salts and metallic 2:1 racemic salt with PF_6^- [5], whereas the use of ClO_4^- proved to be of huge importance across the preparation of the enantiomorphous salts $[(S,S)\text{-}2]_2\text{ClO}_4$ and $[(R,R)\text{-}2]_2\text{ClO}_4$ which allowed the first observation of the electrical magnetochiral anisotropy (eMChA) effect [6,7] in a bulk crystalline chiral conductor [8]. Thus, the addition of a second stereogenic center on the EDT-TTF platform has a paramount importance for the resulting crystalline materials. Interestingly, the use of **2** in combination with AsF_6^- or SbF_6^- , having larger volumes than PF_6^- , favored the formation of metallic enantiopure salts $(2)_2\text{XF}_6$ ($X = \text{As}, \text{Sb}$) as a consequence of the interplay between the anion size, its propensity to engage in intermolecular hydrogen bonding and chirality of the donor [9], with the much larger double octahedral shaped fluorinated dianion $[\text{Ta}_2\text{F}_{10}\text{O}]^{2-}$ semiconducting salts of **2** with a 3:1 stoichiometry having been obtained [10]. In order to develop the families of chiral conducting materials further, a first objective of the present work is directed to the association of the mono-substituted donor **1** with the larger anion AsF_6^- . Secondly, when considering the important role played by the linear monoanion I_3^- in the field of molecular conductors through the synthesis of the first ambient pressure organic superconductor $(\text{BEDT-TTF})_2\text{I}_3$ [11–13], its use in radical cation salts with the donors **1** and **2** has been investigated and described herein. Note that tetramethylbis(ethylenedithio)-tetrathiafulvalene (TM-BEDT-TTF), the first reported enantiopure TTF derivative [14], provided 1:1 semiconducting radical cation salts with I_3^- [15], besides other conducting materials [16–18], thus demonstrating the drastic consequences of the introduction of substituents on the ethylene carbon atoms on the stoichiometry and properties of the resulting materials. Finally, another interesting comparison can be made between the two diastereomers of **2**, i.e., the (*S,S*)/(*R,R*) pair and the *meso* form (Scheme 1). Indeed, radical cation salts based on the related donor dimethyl-bis(ethylenedithio)-tetrathiafulvalene (DM-BEDT-TTF) [19,20], which also presents a similar pair of diastereomers (*S,S*)/(*R,R*) and *meso*, show striking differences between them. For example, with the PF_6^- anion, semiconducting orthorhombic $[(R,R)\text{-DM-BEDT-TTF}]_2\text{PF}_6$ and monoclinic $[(rac)\text{-DM-BEDT-TTF}]_2\text{PF}_6$ salts [21] have been described, while the (*meso*)-DM-BEDT-TTF form provided the triclinic $\beta\text{-}[(meso)\text{-DM-BEDT-TTF}]_2\text{PF}_6$ salt which showed a superconducting transition with $T_c \sim 4.3$ K under 4.0 kbar [22,23]. Thus, the third objective of the present work is to introduce the hitherto unknown (*meso*)-**2** donor and radical cation salts containing, especially, PF_6^- and ClO_4^- anions, to be compared with the corresponding materials with (*S,S*)/(*R,R*)-**2** [5,8].



Scheme 1. EDT-TTF, Me-EDT-TTF (**1**), DM-EDT-TTF (**2**), BEDT-TTF, TM-BEDT-TTF and DM-BEDT-TTF donors. Specifically, **1** and **2** were used in the present study. Only the (*S*) enantiomers for **1** and **2** together with the (*meso*) form of **2** are represented.

We describe herein a series of radical cation salts of Me-EDT-TTF **1** with the AsF_6^- and I_3^- anions, the complete series of radical cation salts of (*S,S*)/(*R,R*)-**2** with I_3^- and, finally, the synthesis and structural characterization of the new donor (*meso*)-**2** together with its radical cation salts with PF_6^- and XO_4^- ($X = \text{Cl}, \text{Re}$) anions.

2. Results and Discussion

2.1. Radical Cation Salts of Me-EDT-TTF (1) with the AsF_6^- Anion

As outlined in the Introduction, donor **1** provided a complete series of radical cation salts $(1)_2\text{PF}_6$ for which the enantiopure compounds crystallized in the triclinic space group $P1$, with two independent donor molecules and one anion in the unit cell, while the racemic salt crystallized in the triclinic space group $P\bar{1}$ with one independent donor in the asymmetric unit and the anion located on an inversion center [3]. We describe here the analogous complete series of chiral radical cation salts of Me-EDT-TTF **1** with AsF_6^- and compare their structural features and conducting properties with the previously reported PF_6^- counterparts. Donor **1**, prepared according to our published procedure [3], afforded enantiopure and racemic salts by electrocrystallization in THF in the presence of $((n\text{-Bu})_4\text{N})\text{AsF}_6$. Single crystals were obtained in the form of black plates following experimental conditions identical with those employed for the PF_6 series. Note that, with donor **1**, the use of tetrahydrofuran (THF) as an electrocrystallization solvent generally requires working temperatures of 2–3 °C in order to favor crystallization of radical cation salts.

$[(rac)\text{-}1]_2\text{AsF}_6$ is isostructural with the previously described $[(rac)\text{-}1]_2\text{PF}_6$ metallic salt [3], but also with the racemic $[(rac)\text{-}2]_2\text{PF}_6$ [5]. It crystallizes in the triclinic centrosymmetric space group $P\bar{1}$ with one independent donor molecule and half of anion, located on an inversion center, in the asymmetric unit (Figure 1a, Table S1). The ethylene bridge C7–C8 is disordered over two positions A and B with s.o.f. values of 0.62 and 0.38, respectively, whereas the methyl group C9 is not disordered and adopts an equatorial conformation, thus leading to the presence of both enantiomers (*S*) and (*R*) on the same crystallographic site. The four equatorial fluorine atoms are disordered on two positions each. The enantiopure salts $[(S)\text{-}1]_2\text{AsF}_6$ and $[(R)\text{-}1]_2\text{AsF}_6$ crystallize in the non-centrosymmetric triclinic space group $P1$ with two independent donor molecules and one anion in the asymmetric unit (Figure 1b for the (*S*) enantiomer). Since they are isostructural, only the structure of $[(S)\text{-}1]_2\text{AsF}_6$ will be detailed.

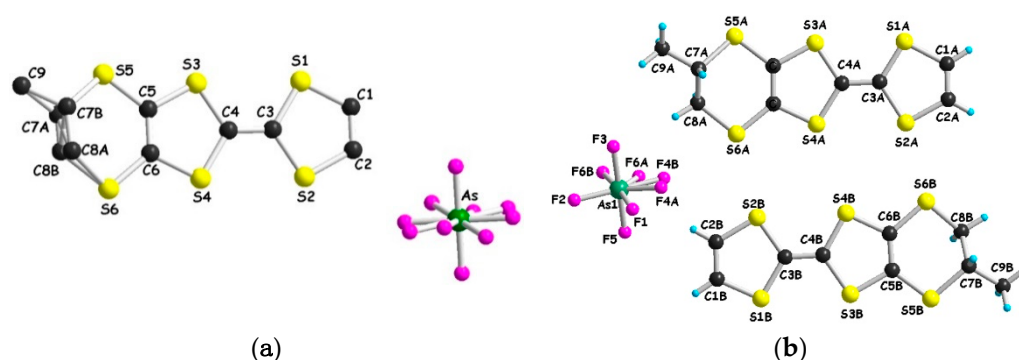


Figure 1. (a) Molecular structure of $[(rac)\text{-}1]_2\text{AsF}_6$. H atoms have been omitted for clarity. Equatorial F atoms are disordered on two positions each (s.o.f. 0.66 and 0.34). The ethylene bridge is disordered over two positions A (s.o.f. 0.62) and B (s.o.f. 0.38); (b) Molecular structure of $[(S)\text{-}1]_2\text{AsF}_6$. F4 and F6 atoms are disordered (s.o.f. 0.57 and 0.43).

Contrary to the racemic form, the donor molecules of the enantiopure salts have no occupational disorder; the methyl substituent adopts equatorial conformation in both independent molecules, and two of the fluorine atoms were modelled over two positions.

The lengths of the central C = C bond together with the internal C–S bonds, shown in Table 1 for $[(rac)\text{-}1]_2\text{AsF}_6$ and $[(S)\text{-}1]_2\text{AsF}_6$, are in agreement with a +0.5 oxidation state of the donor and are comparable with the values measured for the $[(rac)\text{-}1]_2\text{PF}_6$ salt [3].

Table 1. Selected C = C and C–S internal bond distances for [(*rac*)-1]₂AsF₆ and [(*S*)-1]₂AsF₆.

Bond lengths (Å)				
		[(<i>S</i>)-1] ₂ AsF ₆	[(<i>rac</i>)-1]AsF ₆	
A	C3A–C4A	1.367(9)	C3–C4	1.363(5)
	S1A–C3A	1.714(7)	S1–C3	1.739(4)
	S2A–C3A	1.759(7)	S2–C3	1.739(3)
	S3A–C4A	1.744(7)	S3–C4	1.740(3)
	S4A–C4A	1.736(7)	S4–C4	1.733(3)
B	C3B–C4B	1.374(10)		
	S1B–C3B	1.737(7)		
	S2B–C3B	1.753(7)		
	S3B–C4B	1.733(7)		
	S4B–C4B	1.726(7)		

A classical organic-inorganic segregation occurs in the packing of both enantiopure and racemic salts, with the donors adopting a β -type organization in parallel columns, with short intrastack and interstack S \cdots S distances (Figure 2a and Figure S1). As in the case of the PF₆[−] homologous series, the donors engage in a complex set of intermolecular CH \cdots F hydrogen bond interactions with the fluorine atoms of the anion (Figure 2b and Figure S2). When comparing the structure of the two series, the CH \cdots F distances, such as those for CH_{vinyl} and CH_{Me}, are either equal or slightly smaller for AsF₆[−] than those with PF₆[−], as a consequence of the longer As–F bond lengths (Tables S2 and S3). All fluorine atoms are involved in such hydrogen-bonding interactions.

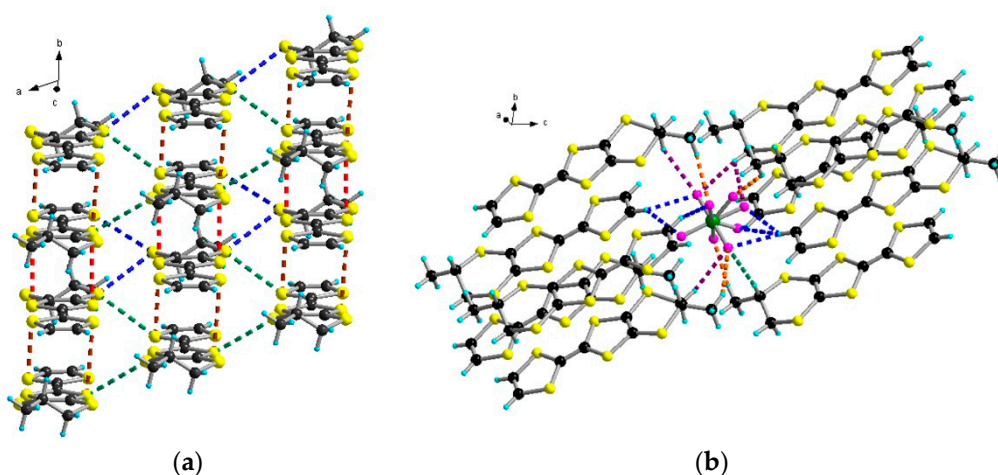


Figure 2. (a) Layer of donors in the packing of [(*S*)-1]₂AsF₆ with an emphasis on the S \cdots S short contacts: red dotted lines (3.55–3.59 Å), brown dotted lines (3.62 Å), blue dotted lines (3.60–3.63 Å) and green dotted lines (3.68–3.70 Å); (b) C–H \cdots F short contacts: blue dotted lines for CH_{vinyl} (2.40–2.44–2.53 Å), orange dotted lines for Me (2.42–2.55 Å), violet dotted lines for CH₂ (2.49–2.66 Å) and green dotted lines for CH_{Me} (2.53 Å).

Thus, this (1)₂AsF₆ series presents the same structural characteristics as the (1)₂PF₆ series and also as the isostructural one of donor 2 with AsF₆[−], namely (2)₂AsF₆ [9]. Since the latter two show metal-like behavior, it is reasonable to envisage similar conducting properties for the former. Although crystals of the series (1)₂AsF₆ were rather small and brittle, single crystal resistivity measurements could be performed for [(*rac*)-1]₂AsF₆ and [(*R*)-1]₂AsF₆. The metallic behavior in the high-temperature regime could not be detected,

as in the case of two point contact measurements in the $(1)_2\text{PF}_6$ series, in spite of rather high values of the room temperature conductivities ($\sigma_{\text{RT}} \approx 1\text{--}10 \text{ S cm}^{-1}$) and very small activation energies (9–12 meV) (Figure 3a). Most likely, the presence of structural disorder on the donors and the anions prevents the observation of a metal-like conductivity. However, thermoelectric power measurements suggest metallic behavior in the high-temperature regime according to the small positive values of the Seebeck coefficient decreasing towards zero upon cooling (Figure 3b).

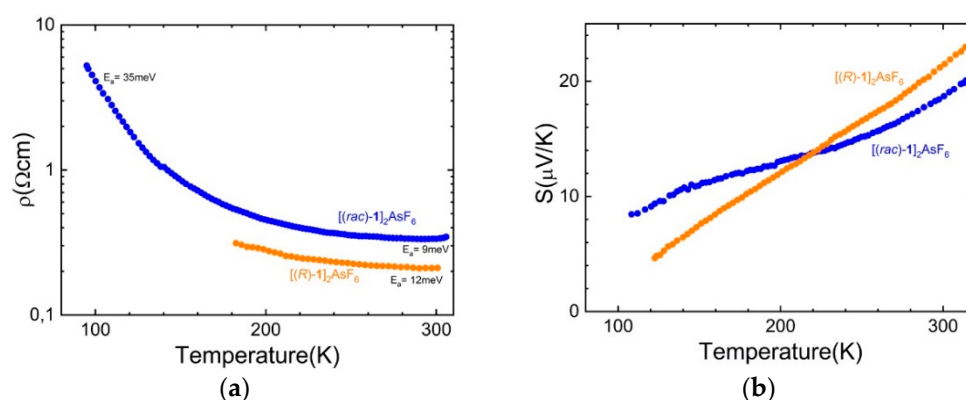


Figure 3. (a) Temperature dependence of the electrical resistivity ρ for single crystals of $[(\text{rac})\text{-}1]_2\text{AsF}_6$ (blue curve) and $[(\text{R})\text{-}1]_2\text{AsF}_6$ (orange curve) measured using four-in-line contacts; (b) Temperature dependence of the thermoelectric power for a single crystal of $[(\text{rac})\text{-}1]_2\text{AsF}_6$ (blue curve) and $[(\text{R})\text{-}1]_2\text{AsF}_6$ (orange curve).

These values of conductivity are comparable to those in the PF_6^- series; moreover, no striking difference has been observed between the racemic and enantiopure materials. This last feature is not really surprising in view of the similar packing of the donors, although one might argue that the enantiopure salts could show in principle higher conductivity since there is no structural disorder on the donors. However, the anion is disordered in all the salts of the series; therefore, this feature can hamper such fine observations.

Surprisingly, in a second set of experiments realized with the enantiopure donor and $[(n\text{-Bu})_4\text{N}]\text{AsF}_6$ in separate compartments, totally different 1:1 salts crystallized in the anodic compartment as black prismatic blocks. Once again, a working temperature of 2–3 °C was imposed in order to obtain crystalline materials. Accordingly, $[(\text{S})\text{-}1]\text{AsF}_6 \cdot \text{C}_4\text{H}_8\text{O}$ and $[(\text{R})\text{-}1]\text{AsF}_6 \cdot \text{C}_4\text{H}_8\text{O}$ radical cation salts are isostructural and crystallize in the triclinic system non-centrosymmetric system $P1$, with two independent donors A and B, two anions and two tetrahydrofuran (THF) molecules in the unit cell (Figure 4 and Figure S3 for the (R) enantiomer, Table S4).

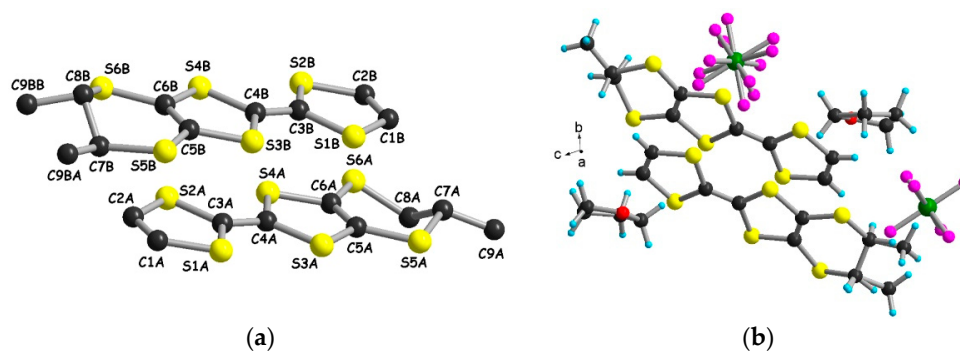


Figure 4. (a) The two independent donor molecules in the crystal structure of $[(\text{S})\text{-}1]\text{AsF}_6 \cdot \text{C}_4\text{H}_8\text{O}$. C9B atom is disordered over two positions A (s.o.f. 0.69) and B (s.o.f. 0.31). H atoms have been omitted for clarity; (b) Molecular structure of $[(\text{S})\text{-}1]\text{AsF}_6 \cdot \text{C}_4\text{H}_8\text{O}$. F1B–F6B atoms are disordered over two positions A (s.o.f. 0.57) and B (s.o.f. 0.43).

In one of the two donors, the methyl substituent C9B, located in an equatorial position, is disordered over two positions (C9BA and C9BB), which is different to the previous mixed-valence salts. Moreover, all the six fluorine atoms of one anion are disordered on two positions each. The stoichiometry of the two compounds indicates that both independent donors are in a radical cation state, in agreement with the values of the central C = C and internal C–S bond lengths (Table 2). The crystallization of these 1:1 phases is very likely favored by the much lower concentration of available AsF_6^- counter ion in the anodic compartment, leading to the complete oxidation of the donors before crystallization.

Table 2. Selected C = C and C–S internal bond distances for $[(S)-1]_2\text{AsF}_6$ and $[(R)-1]_2\text{AsF}_6$.

Bond Lengths (Å)				
		$[(S)-1]\text{AsF}_6 \cdot \text{C}_4\text{H}_8\text{O}$	$[(R)-1]\text{AsF}_6 \cdot \text{C}_4\text{H}_8\text{O}$	
A	C3A–C4A	1.396(13)	C3A–C4A	1.4214(13)
	S1A–C3A	1.737(9)	S1A–C3A	1.734(12)
	S2A–C3A	1.710(10)	S2A–C3A	1.7068(98)
	S3A–C4A	1.705(9)	S3A–C4A	1.6963(91)
	S4A–C4A	1.727(9)	S4A–C4A	1.7142(12)
B	C3B–C4B	1.389(13)	C3B–C4B	1.3577(13)
	S1B–C3B	1.729(10)	S1B–C3B	1.7306(89)
	S2B–C3B	1.710(10)	S2B–C3B	1.7154(12)
	S3B–C4B	1.705(10)	S3B–C4B	1.7128(12)
	S4B–C4B	1.735(9)	S4B–C4B	1.7485(88)

As is often observed in the case of salts based on fully oxidized donors, the radical cations form strong eclipsed dimers in the packing, with very short S...S intradimer distances of 3.33–3.37 Å and much longer lateral S...S interdimer distances (3.59–3.77 Å) (Figure 5a). The dimers are separated along the stacking direction by THF molecules (Figures S4 and S5 for the *(R)* enantiomer). The fluorine atoms are engaged in hydrogen bonding with protons of the donors but also with a CH_2 group of THF, thus providing a certain stability of the crystals against the desolvation (Figure 5b and Figure S6 for the *(R)* enantiomer, Tables S5 and S6). When considering this strong dimerization of the donors, it can be safely concluded that the two salts are insulators.

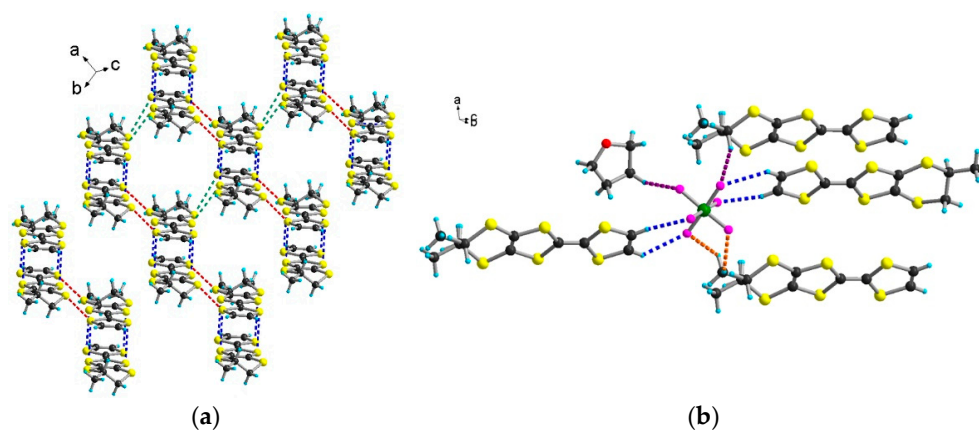


Figure 5. (a) Packing of the donors in the structure of $[(S)-1]\text{AsF}_6 \cdot \text{C}_4\text{H}_8\text{O}$ with emphasis on the S...S short contacts: blue dotted lines for (3.33–3.37 Å), red dotted lines for (3.59–3.66 Å), green dotted lines for (3.75–3.77 Å); (b) View of the structure of $[(S)-1]\text{AsF}_6 \cdot \text{C}_4\text{H}_8\text{O}$ with an emphasis on the C–H...F short contacts: blue dotted lines for CH_{vinyl} (2.41–2.64 Å), orange dotted lines for Me (2.59–2.62 Å), violet dotted lines for CH_2 and CH (2.64–2.65 Å).

2.2. Radical Cation Salts of Me-EDT-TTF (1) and DM-EDT-TTF (2) with the I_3^- Anion

As mentioned above, TM-BEDT-TTF afforded 1:1 radical cation salts with the tris(iodide) anion I_3^- [15]. On the other hand, BEDT-TTF provided the ambient pressure superconducting phase $(BEDT-TTF)_2I_3$ [11–13], while a 1:1 salt was described with EDT-TTF [24]. Here, we present our results on the complete series of radical cation salts of chiral EDT-TTF derived donors 1 and 2 with the I_3^- anion. The crystalline salts, collected as brown plates for 1 and black prisms for 2, were prepared by electrocrystallization of the respective donors in acetonitrile at 20 °C in the presence of $[(n-Bu)_4N]I_3$.

The racemic and enantiopure salts $(1)I_3$ are isostructural, with $[(rac)-1]I_3$ crystallizing in the centrosymmetric triclinic $P\bar{1}$ space group, while the enantiopure $[(S)-1]I_3$ and $[(R)-1]I_3$ are in the non-centrosymmetric triclinic space group $P1$ (Table S7). The asymmetric unit consists of two independent donor molecules and two anions for the latter (Figure 6a for $[(S)-1]I_3$) and one donor and two half anions for the former. In both independent molecules of $[(S)-1]I_3$, the methyl substituent (C9A and C9B) adopts an axial position. The central C = C bond lengths values, together with the internal C–S bond lengths (Table S8), are indicative of the +1 oxidation state, in agreement with the 1:1 stoichiometry.

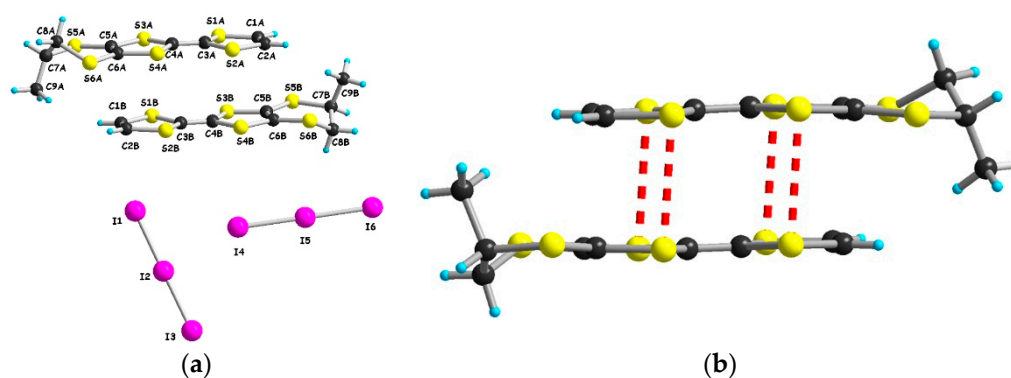


Figure 6. (a) Molecular structure of $[(S)-1]I_3$ together with the atom numbering scheme; (b) Dimer motif in the structure of $[(S)-1]I_3$ with emphasis on the $S\cdots S$ short contacts: red dotted lines for 3.34, 3.37, 3.38 and 3.42 Å.

The donors A and B are strongly dimerized as attested by the eclipsed arrangement and the very short intradimer $S\cdots S$ distances ranging between 3.34 and 3.42 Å (Figure 6b for $[(S)-1]I_3$). The packing of the donors is strongly reminiscent of the one observed in the structure of $(EDT-TTF)I_3$ [24]. Accordingly, one I_3^- anion separates the layers of donors, and the other I_3^- anion is embedded in the layer, with its axis parallel to the long axis of the donors, thus leading to only lateral overlap between the dimers (Figure 7 for $[(R)-1]I_3$).

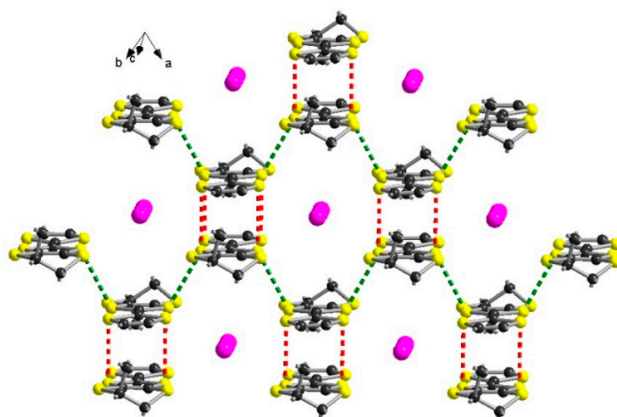


Figure 7. Packing of donors in the structure of $[(R)-1]I_3$ with emphasis on the $S\cdots S$ contacts shorter than 3.6 Å: red dotted lines for 3.33, 3.35 and 3.39 Å; green dotted lines for 3.45 and 3.48 Å.

Although the interdimer S...S distances for these lateral donor...donor contacts are as short as 3.45–3.48 Å (Figure 7), one can expect very weak conductivity for these radical cation salts of 1:1 composition when considering the strong dimerization of the donors.

Thus, within this series of (1)I₃, the presence of a methyl substituent on the ethylene bridge of EDT-TTF as in donor 1 does not have a strong impact on the packing, which is similar to the one observed in the parent (EDT-TTF)I₃ salt. What would be the consequence of introducing a second methyl substituent as in donor 2? Accordingly, we have proceeded to electrocrystallization experiments of 2 in the presence of [(*n*-Bu)₄N]I₃ in similar conditions as for 1. A complete series of isostructural crystalline radical cation salts formulated as (2)I₃ has been obtained as well, with the racemic compound having crystallized in the triclinic space group *P*-1 and the enantiopure counterparts in triclinic *P*1 (Table S9). The asymmetric unit of the former contains one independent donor and one anion, while those of the latter contain two independent donors and two anions. In contrast to the previous series based on donor 1, now both tris(iodide) ions are aligned with the long axis of the donors, and the methyl groups are located in equatorial positions (eq, eq) (Figure 8).

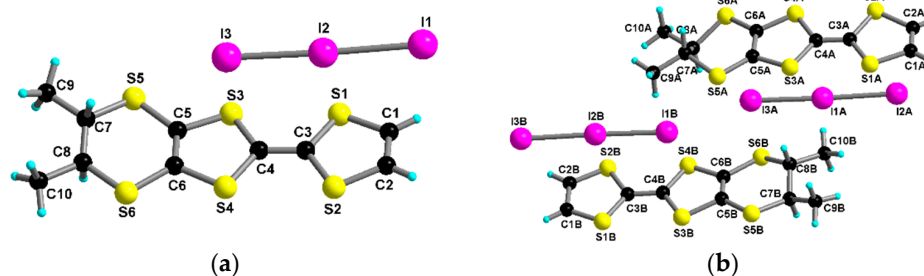


Figure 8. (a) Molecular structure of [(*rac*)-2]I₃ with together with the atom numbering scheme; (b) Molecular structure of [(*R,R*)-2]I₃ together with the atom numbering scheme.

As it was recently evidenced by DFT calculations, the difference in energy between the axial and equatorial conformers of DM-EDT-TTF amounts only to ≈ 3 kcal mol⁻¹ [25], and even less for the monomethylated precursors [26], the occurrence of one form or the other in the solid state being determined mainly by the packing and establishment of intermolecular interactions. The analysis of the central C = C and internal C–S bonds lengths values allows the assignment of the oxidation state +1 to the donors, in agreement with the 1:1 stoichiometry. Since in this case both tris(iodide) anions are aligned with the long axis of the donors, the *c* direction, along which no donor...donor interaction takes place (Figures S7 and S8), mixed donor/anion layers are formed in the *ab* plane, with strongly dimerized donors interacting laterally (Figure 9a for (*rac*) and Figure 9b for (*R,R*)).

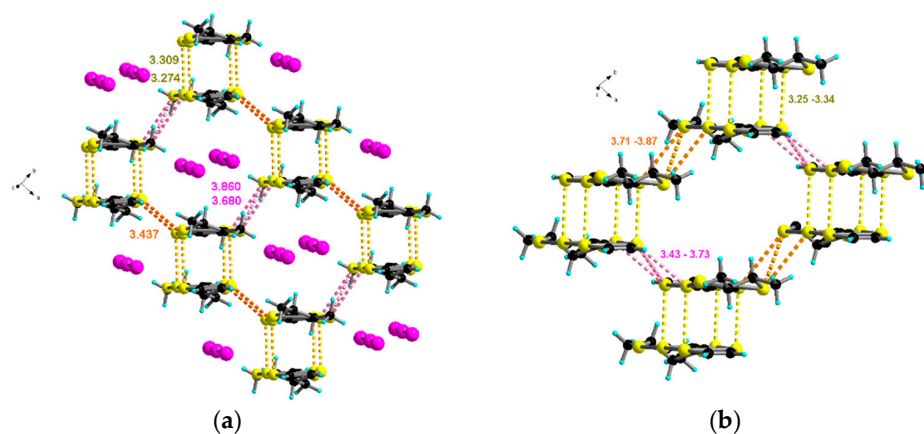
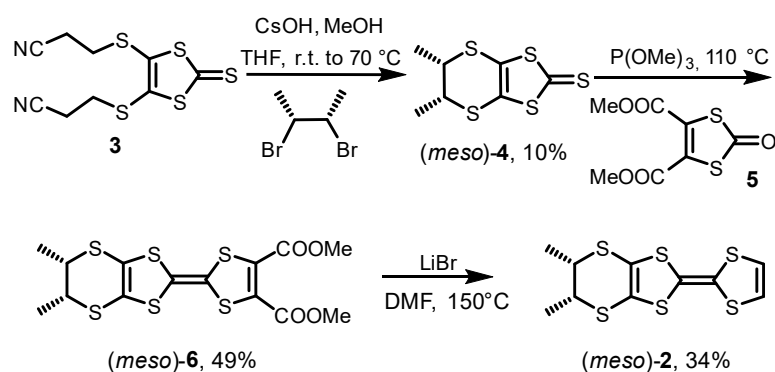


Figure 9. (a) Packing of the donors and highlight of the S...S short contacts for [(*rac*)-2]I₃; (b) Packing of the donors and highlight of the S...S short contacts for [(*R,R*)-2]I₃. The anions are not shown.

The intradimer S...S distances of 3.27–3.31 Å for [(*rac*)-2]I₃ and 3.25–3.34 Å for [(*R,R*)-2]I₃ are even shorter than in the previous series, probably as a consequence of the (eq, eq) conformation of the methyl groups, while the interdimer ones are slightly longer (Figure 9 and Figure S9). Once again, due to the strong dimerization, the conductivity of these materials is expected to be poor.

2.3. Synthesis and Structure of (*meso*)-DM-EDT-TTF

The fascinating properties shown by the radical cation salts of DM-EDT-TTF (**2**) in its chiral version, that is (*rac*), (*S,S*) and (*R,R*) forms, with different anions (ClO₄[−] [8], PF₆[−] [5], AsF₆[−] [9], SbF₆[−] [9], Ta₂F₁₀O [10]) prompted us to investigate the hitherto unknown (*meso*) form of DM-EDT-TTF ((*meso*)-**2** in Scheme 1). For its preparation, we have envisaged a three-step procedure, starting with a double nucleophilic substitution of (*meso*)-2,3-dibromobutane with dmit^{2−}, generated from the protected precursor **3** in basic conditions, to form (*meso*)-DM-DDDT **4**. Then, a classical phosphite-mediated cross-coupling reaction of **4** with the dicarboxylate dithiolene **5** afforded the TTF (*meso*)-**6**, which was subsequently heated in DMF in the presence of lithium bromide to yield (*meso*)-**2** upon a double decarboxylation (Scheme 2).



Scheme 2. Synthesis of (*meso*)-DM-EDT-TTF donor ((*meso*)-**2**).

The neutral donor (*meso*)-**2** crystallizes in the monoclinic centrosymmetric space group $P2_1/n$, with one independent molecule in the unit cell (Table S11). The dithiine six-membered ring shows a sofa-type conformation (dihedral angles C5–C6–S6–C7 and C6–C5–S5–C8 measure 5.05° and 23.2°, respectively), with axial (C10) and equatorial (C9) orientations of the methyl substituents (Figure 10) and boat-like conformation of the TTF unit. Central C=C and internal C–S bond distances have typical values for neutral donors (Table S12). In the packing, the donors organize in orthogonal dyads (Figure S10), with intermolecular S...S contacts of 3.54–3.87 Å.

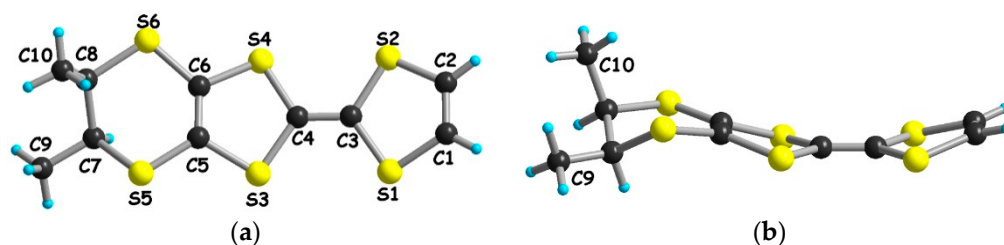


Figure 10. (a) Molecular structure of (*meso*)-**2**; (b) Lateral view.

2.4. Radical Cation Salts of (*meso*)-DM-EDT-TTF

Our prime objective was to obtain radical cation salts of (*meso*)-**2** with PF₆[−] and ClO₄[−] anions in order to compare them with those obtained with donors **1** and **2** (chiral form), previously reported. Accordingly, electrocrystallization of (*meso*)-**2** in the presence

of $[(n\text{-Bu})_4\text{N}]\text{PF}_6$ and $[(n\text{-Bu})_4\text{N}]\text{ClO}_4$ provided 1:1 radical cation salts $[(\text{meso})\text{-2}]\text{PF}_6$ and $[(\text{meso})\text{-2}]\text{ClO}_4$, respectively, as black crystalline needles. Additionally, knowing that ClO_4^- and ReO_4^- anions usually afford isostructural salts, the use of $[(n\text{-Bu})_4\text{N}]\text{ReO}_4$ leads to the formation of crystalline $[(\text{meso})\text{-2}]\text{ReO}_4$, isostructural with its perchlorate congener (Table S11). A working temperature of 3 °C had to be imposed in the case of ClO_4^- and ReO_4^- salts, very likely because of the use of THF as co-solvent.

$[(\text{meso})\text{-2}]\text{PF}_6$ crystallizes in the monoclinic centrosymmetric space group $P2_1/n$, with one independent donor molecule and one anion in the unit cell (Figure 11a). While in the chiral form of **2**, the methyl substituents can adopt either axial (ax) or equatorial (eq) conformations, the most common being the equatorial one in radical cation salts, thus maximizing the overlap between the donors, in $(\text{meso})\text{-2}$ the conformation is necessarily (ax, eq). In the packing, an organic-inorganic segregation takes place along the c direction, with the donors forming strong centrosymmetric dimers, as attested by the short intermolecular $\text{S}\cdots\text{S}$ contacts of 3.35–3.37 Å (Figure 11b). The dimers interact only laterally in the ab plane, yet with much longer $\text{S}\cdots\text{S}$ contacts (3.64–3.81 Å). A network of hydrogen bonding exists between fluorine atoms and the different hydrogen atoms of the donor: $\text{H}_{\text{vinyl}}\cdots\text{F}$ (2.32–2.36 Å) and $\text{H}_{\text{Me}}\cdots\text{F}$ (2.53–2.75 Å), $\text{H}_{\text{CH}}\cdots\text{F}$ (2.45–2.65 Å) (Figure S11).

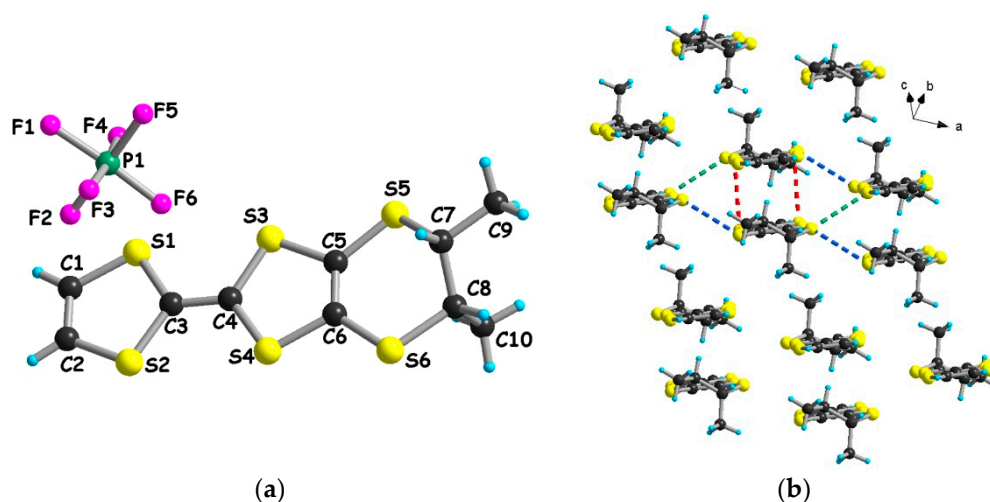


Figure 11. (a) Molecular structure of $[(\text{meso})\text{-2}]\text{PF}_6$; (b) Packing diagram for $[(\text{meso})\text{-2}]\text{PF}_6$ with $\text{S}\cdots\text{S}$ short contacts highlighted. Red dotted lines (3.35–3.37 Å), blue dotted lines (3.75–3.81 Å), green dotted lines (3.64–3.68 Å). The anions are not shown.

As mentioned above, $[(\text{meso})\text{-2}]\text{ClO}_4$ and $[(\text{meso})\text{-2}]\text{ReO}_4$ are isostructural, crystallizing in the triclinic centrosymmetric space group $P\bar{1}$, with one independent donor and one anion in the unit cell (Figures S12 and S13, Table S11). The donors organize in dyads, through short $\text{S}\cdots\text{S}$ interactions (3.34–3.41 Å), further interacting laterally (Figure 12a), while donors-anions' segregation establishes along the c direction (Figure 12b and Figure S14). The lateral $\text{S}\cdots\text{S}$ contacts are on average shorter in the ClO_4^- and ReO_4^- salts than in the PF_6^- one.

A strong dimerization of radical cations, with little interdimer interactions, is generally detrimental for good electron transport properties. Indeed, single crystal resistivity measurements for $[(\text{meso})\text{-2}]\text{PF}_6$ and $[(\text{meso})\text{-2}]\text{ReO}_4$ show semiconducting behavior with room temperature conductivities σ_{RT} of $1.4 \cdot 10^{-5} \text{ S cm}^{-1}$ for the former and $1.6 \cdot 10^{-4} \text{ S cm}^{-1}$ for the latter, the activation energies E_a being around 300–340 meV (Figure 13). The origin of the higher conductivity of the ReO_4^- salt compared to the PF_6^- salt may be in the stronger lateral interdimer interactions observed in the former.

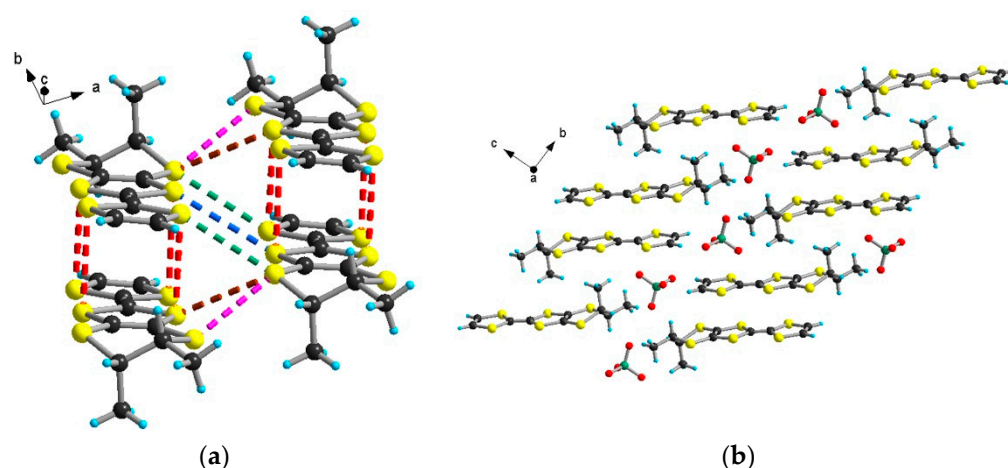


Figure 12. (a) Packing diagram for $[(\text{meso})\text{-}2]\text{ClO}_4$ in the ab plane with an emphasis on short $\text{S}\cdots\text{S}$ interactions. Red dotted lines (3.34–3.41 Å), green dotted lines (3.49 Å), blue dotted lines (3.79 Å), magenta lines (3.48 Å), brown lines (3.65 Å); (b) Packing diagram in the bc plane showing the donors-anions' segregation.

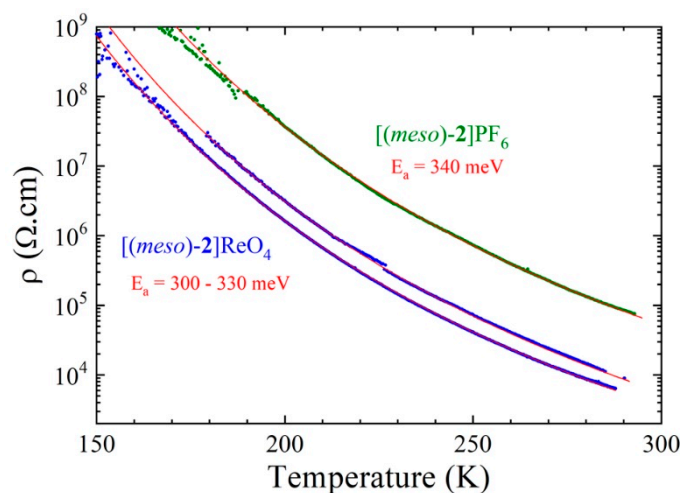


Figure 13. Temperature dependence of the electrical resistivity ρ for one single crystal of $[(\text{meso})\text{-}2]\text{PF}_6$ (green curve) and two single crystals of $[(\text{meso})\text{-}2]\text{ReO}_4$ (blue curves) measured using two contacts. The red lines are the fit to the activation law $\rho = \rho_0 \exp(E_a/T)$ in the 160–300 K temperature range giving the activation energy E_a .

Across the preparation and conducting properties of these radical cation salts based on $(\text{meso})\text{-}2$, it is clear that the mutual orientation of the methyl substituents on the ethylene bridge plays a paramount role on the donor:anion stoichiometry and the packing of the donors. Indeed, in $(\text{meso})\text{-}2$, one of the methyl substituents is necessarily axial, thus precluding strong axial overlap between donors, at the difference with $(S,S)\text{-}2$ and $(R,R)\text{-}2$ where both methyl groups are equatorial in the most conducting salts.

3. Conclusions

In the continuation of our research lines on chiral materials and, more specifically, on chiral molecular conductors, we reported here a new series of radical cation salts based on the chiral donors Me-EDT-TTF (**1**) and DM-EDT-TTF (**2**) as racemic and enantiopure forms, obtained by electrocrystallization. The former provided mixed valence salts $(\mathbf{1})_2\text{AsF}_6$ with metal-like behavior in the high-temperature regime, which are isostructural with the previously described PF_6 counterpart, but also with the $(\mathbf{2})_2\text{AsF}_6$ series. Additionally, 1:1 enantiopure salts formulated as $[(S)\text{-}1]\text{AsF}_6 \cdot \text{C}_4\text{H}_8\text{O}$ and $[(R)\text{-}1]\text{AsF}_6 \cdot \text{C}_4\text{H}_8\text{O}$ have been

obtained in slightly different conditions. With the tris(iodide) anion I_3^- , both donors afforded 1:1 salts, i.e., (1) I_3 and (2) I_3 , as racemic and enantiopure forms, yet the disposition of the anions with respect to the donors is drastically different in the two series. Finally, the synthesis, characterization and single crystal X-ray structure of the new donor (*meso*)-2 are described, together with its poorly semiconducting 1:1 radical cation salts with the PF_6^- , ClO_4^- and ReO_4^- anions. The striking difference between the salts formed by (*meso*)-2 and those resulting from the chiral form (*S,S*)/(*R,R*)-2 with the same anions is very likely due to the location of the methyl substituents which is necessarily axial, equatorial in the former, while in the latter they can adopt an equatorial, equatorial conformation, thus maximizing the packing. Throughout these different series of radical cation salts, the importance of the number of stereogenic centers, of their mutual arrangement in the case of (*meso*)-2 and (*S,S*)/(*R,R*)-2 and of the nature of the counter-ion on the donor:anion stoichiometry, packing of the donors and, ultimately, electron transport properties, are highlighted. Future work will be devoted to conductivity measurements under high pressures, and the use of these chiral precursors in electrocrystallization in the presence of magnetic anions. This last direction is particularly interesting when considering the possibility of combining chirality with conducting and magnetic properties [17,27], since in magnetic conductors, the existence of delocalized π -electrons and localized d-electrons may lead to exotic phenomena such as magnetic-field-induced superconductors, magnetoresistance effects and magnetic-field-switchable conductors, with applications in molecular electronics and spintronics [28–32].

4. Materials and Methods

All commercially available reagents and solvents were used as received unless otherwise noted. Dry tetrahydrofuran was directly used from the purification machines. Chloroform as a solvent for synthesis was passed through a short column of basic alumina prior to use. Chromatography purifications were performed on silica gel, and thin layer chromatography (TLC) was carried out using aluminum sheets precoated with silica gel. NMR spectra were acquired on a Bruker Avance DRX 300 spectrometer operating at 300 MHz for 1H at room temperature in $CDCl_3$ solutions. 1H NMR spectra were referenced to the residual protonated solvent (1H). All chemical shifts are expressed in parts per million (ppm) downfield from external tetramethylsilane (TMS) using the solvent residual signal as an internal standard, and the coupling constant values (J) are reported in Hertz (Hz). The following abbreviations have been used: s, singlet; d, doublet; m, multiplet. Mass spectrometry MALDI–TOF MS spectra were recorded on a Bruker Biflex-IIIITM apparatus equipped with a 337-nm N2 laser.

Precursors Me-EDT-TTF 1 [3], (*S,S*)- and (*R,R*)-DM-EDT-TTF 2 [5] were synthesized according to the literature procedures, while the preparation of (*meso*)-2 is described in this report.

(*meso*)-DM-DDDT 4: Compound 3 (4.5 g, 14.8 mmol) was added into a 500 mL Schlenk round bottomed flask under argon, and then dry THF (400 mL) was poured into the flask. After 10 min, a solution of caesium hydroxide (7 g, 41.6 mmol) in dry methanol (50 mL) was added dropwise, and the color started to turn violet. Then, the resulting solution was left under stirring for one hour at room temperature, followed by the addition of (*meso*)-2,3-dibromobutane (5.5 g, 25 mmol) and reflux for one night. After cooling to room temperature, the solvent was removed under vacuum, and the solid residue was extracted twice with DCM and water (250/500 mL). The combined organic phases were concentrated, and the residue was purified by column chromatography (petroleum ether/DCM 8:2) to give compound 4 (0.36 g, 10%); 1H NMR (300 MHz, $CDCl_3$): δ 3.57 (m, 2H, -SCH), 1.36 (d, 6H, -CH₃) ppm.

(*meso*)-DM-EDT-TTF-(COOMe)₂ 6: Compound 4 (0.3 g, 1.19 mmol) and dimethyl 2-oxo-1,3-dithiole-4,5-dicarboxylate 5 (0.6 g, 2.5 mmol) were mixed under argon in freshly distilled trimethyl phosphite (10 mL), and the mixture was heated at 110 °C for 5 h. After this period, the solvent was evaporated in a rotary evaporator, and then toluene (20 mL)

was added and evaporated. The last procedure was repeated twice. The product was solubilized in dichloromethane and passed through a silica column to remove the remaining phosphite and then purified by chromatography using petroleum spirit/dichloromethane 1/1 to afford a red-brown solid (0.255 g, 49%); ^1H NMR (300 MHz, CDCl_3) δ ppm: 3.83 (s, 6H, $-\text{OCH}_3$), 3.54 (m, 2H, $-\text{SCH}$), 1.36 (d, 6H, $-\text{CH}_3$); MS (MALDI-TOF) m/z : 437.4 ($M_{\text{th}} = 437.92$).

(*meso*)-DM-EDT-TTF (*meso*)-1: Compound 6 (0.25 g, 0.57 mmol) and LiBr (0.75 g, 8.6 mmol) were mixed in dimethylformamide (25 mL). The solution was stirred at 150 °C for 30 min, the formation of the product being monitored by TLC. The product was extracted with dichloromethane, and the organic phase was washed with brine and water and then dried over MgSO_4 . The solvent was removed under vacuum, and the product was purified by chromatography on a silica gel column with petroleum spirit/dichloromethane 6/4 to afford a red solid (62 mg, 34 %); ^1H NMR (300 MHz, CDCl_3) δ ppm: 6.32 (s, 2H, $-\text{SCH}=\text{C}$), 3.54 (m, 2H, $-\text{SCH}$), 1.36 (d, 6H, $-\text{CH}_3$); MS (MALDI-TOF) m/z : 321.89 ($M_{\text{th}} = 321.91$).

(1) $_2\text{AsF}_6$: Single crystals of (1) $_2\text{AsF}_6$ (*rac*), (*S*) and (*R*) were obtained by electrocrystallization. The electrolyte solution was prepared from 34.9 mg (5 eq.) of $[(n\text{-Bu})_4\text{N}]\text{AsF}_6$ dissolved in 12 mL of tetrahydrofuran. The anodic chamber was filled with 5 mg of the corresponding donor dissolved in 6 mL of the previously prepared electrolyte solution, whereas the rest of the electrolyte solution (6 mL) was added in the cathodic compartment of the electrocrystallization cell. Single crystals, as black crystalline plates, of the salts were grown at 2–3 °C over a period of 5 days on a platinum wire electrode by applying a constant current of 1 μA .

(1) $\text{AsF}_6 \cdot \text{C}_4\text{H}_8\text{O}$: Single crystals of (1) $\text{AsF}_6 \cdot \text{C}_4\text{H}_8\text{O}$ (*S*) and (*R*) were obtained by electrocrystallization. The electrolyte solution was prepared from 34.9 mg (5 eq.) of $[(n\text{-Bu})_4\text{N}]\text{AsF}_6$ dissolved in 6 mL of tetrahydrofuran. The anodic chamber was filled with 5 mg of the corresponding donor dissolved in 6 mL of tetrahydrofuran, and the previously prepared electrolyte solution was added in the cathodic compartment of the electrocrystallization cell. Single crystals, as black crystalline plates, of the salt were grown at 2–3 °C over a period of 4 to 6 days on a platinum wire electrode by applying a constant current of 1 μA .

(1) I_3 : 20 mg of $[(n\text{-Bu})_4\text{N}]\text{I}_3$ were dissolved in 6 mL of acetonitrile, and the solution was poured in the cathodic compartment of an electrocrystallization cell. The anodic chamber was filled with 5 mg of the donor dissolved in 6 mL of acetonitrile. Single crystals of the salts $[(rac)\text{-}1]\text{I}_3$, $[(S)\text{-}1]\text{I}_3$ and $[(R)\text{-}1]\text{I}_3$ were grown at 20 °C over a period of two weeks on a platinum wire electrode by applying a constant current of 0.5 μA . Black crystalline plates were grown on the electrode.

(2) I_3 : Single crystals of (2) I_3 (*rac*), (*S,S*) and (*R,R*) were obtained by electrocrystallization. The electrolyte solution was prepared from 48.3 mg (5 eq.) of $[(n\text{-Bu})_4\text{N}]\text{I}_3$ dissolved in 12 mL of acetonitrile/chloroform 1/1. The anodic chamber was filled with 5 mg of the corresponding donor dissolved in 6 mL of the previously prepared electrolyte solution, whereas the rest of the electrolyte solution (6 mL) was added in the cathodic compartment of the electrocrystallization cell. Single crystals of the salts, as black crystalline blocks, were grown at 20 °C over a period of 5 days on a platinum wire electrode by applying a constant current of 1 μA .

$[(meso)\text{-}2]\text{PF}_6$: 20 mg of $[(n\text{-Bu})_4\text{N}]\text{PF}_6$ were dissolved in 6 mL CHCl_3 , and then the solution was poured into the cathodic compartment of an electrocrystallization cell. The anodic chamber was filled with 5 mg of $[(meso)\text{-}2]$ dissolved in 6 mL CHCl_3 . Single crystals of the salt were grown at 20 °C over a period of one week on a platinum wire electrode, by applying a constant current of 0.5 μA . Black crystalline needles were collected on the electrode.

$[(meso)\text{-}2]\text{ClO}_4$: 20 mg of $[(n\text{-Bu})_4\text{N}]\text{ClO}_4$ were dissolved in 6 mL of a mixture of 1,1,2-trichloroethane: tetrahydrofuran 1:1, and then the solution was poured in the cathodic compartment of an electrocrystallization cell. The anodic chamber was filled with 5 mg of $[(meso)\text{-}2]$ dissolved in 6 mL of a mixture of 1,1,2-trichloroethane/tetrahydrofuran 1/1.

Single crystals of the salt were grown at 3 °C over a period of one week on a platinum wire electrode by applying a constant current of 1 μ A. Black crystalline needles were grown on the electrode.

[(*meso*)-2]ReO₄: The same procedure as previously was applied by using 20 mg of [(*n*-Bu)₄N]ReO₄ instead of [(*n*-Bu)₄N]ClO₄. Black crystalline needles were grown on the electrode.

Details about data collection and solution refinement are given in Tables S1, S4, S7, S9 and S11. Single crystals of the compounds were mounted on glass fibre loops using a viscous hydrocarbon oil to coat the crystal and then transferred directly to cold nitrogen stream for data collection. X-ray data collection was performed at 150 K on an Agilent Supernova with CuK α (λ = 1.54184 Å). The structures were solved by direct methods with the SHELXS-97 and SIR92 programs and refined against all F² values with the SHELXL-97 program using the WinGX graphical user interface. All non-H atoms were refined anisotropically. Hydrogen atoms were introduced at calculated positions (riding model), included in structure factor calculations but not refined. Crystallographic data for the structures have been deposited with the Cambridge Crystallographic Data Centre, deposition numbers CCDC 2085699 [(*rac*)-1]₂AsF₆, 2085700 [(*S*)-1]₂AsF₆, 2085701 [(*R*)-1]₂AsF₆, 2085702 [(*S*)-1]AsF₆·C₄H₈O, 2085703 [(*R*)-1]AsF₆·C₄H₈O, 2085704 [(*rac*)-1]I₃, 2085705 [(*S*)-1]I₃, 2085706 [(*R*)-1]I₃, 2085707 [(*rac*)-2]I₃, 2085708 [(*S,S*)-2]I₃, 2085709 [(*R,R*)-2]I₃, 2085710 [(*meso*)-2], 2085711 [(*meso*)-2]ClO₄, 2085712 [(*meso*)-2]PF₆ and 2085713 [(*meso*)-2]ReO₄. These data can be obtained free of charge from CCDC, 12 Union road, Cambridge CB2 1EZ, UK (e-mail: deposit@ccdc.cam.ac.uk or <http://www.ccdc.cam.ac.uk>).

Thermoelectric power and electrical conductivity measurements for [(*rac*)-1]₂AsF₆ and [(*R*)-1]₂AsF₆ were made along the longer axis of the crystals in the temperature range of 100–310 K. The measurement cell used was attached to the cold stage of a closed cycle helium refrigerator. The thermopower was measured using a slow AC (ca. 10⁻² Hz) technique [33], by attaching two \varnothing = 25 μ m diameter 99.99% pure Au wires (Goodfellow), thermally anchored to two quartz blocks, with Pt paint (Demetron 308A) to the extremities of an elongated sample using a previously described apparatus [34], controlled by a computer [35]. The oscillating thermal gradient was kept below 1 K and was measured with a differential Au-0.05 at. % Fe vs. chromel thermocouple. The absolute thermoelectric power of the samples was obtained after correction for the absolute thermopower of the Au leads by using the data of Huebener [36]. Electrical resistivity measurements were conducted in a four-in-line contact configuration where a low-frequency AC method (77 Hz) was used; the measurements were conducted with a SRS Model SR83 lock-in amplifier, and a 5 μ A current was applied. Electrical resistivity of [(*meso*)-2]PF₆ and [(*meso*)-2]ReO₄ was measured in two points on needle-shaped single crystals 0.5 mm long. Gold wires were glued with silver paste on gold-evaporated contacts. Different techniques were used to measure resistivity, either applying a constant voltage (1–5 V) and measuring the current with a Keithley 486 or applying a DC current (0.1–0.01 μ A) and measuring the voltage with a Keithley 2400. We have checked for each crystal that both techniques give the same resistance value at room temperature. A low temperature was provided by a homemade cryostat equipped with a 4 K pulse-tube.

Supplementary Materials: The following are available online at <https://www.mdpi.com/article/10.3390/magnetochemistry7060087/s1>: Figure S1: Layer of donors in the packing of [(*rac*)-1]₂AsF₆; Figure S2: C–H···F short contacts in the packing of [(*rac*)-1]₂AsF₆; Figure S3: View of the ordered donor molecule and anion in the crystal structure of [(*R*)-1]AsF₆·C₄H₈O; Figure S4: Packing of the donors in the structure of [(*S*)-1]AsF₆·C₄H₈O; Figure S5: Packing of the donors in the structure of [(*R*)-1]AsF₆·C₄H₈O; Figure S6: View of the structure of [(*R*)-1]AsF₆·C₄H₈O; Figure S7: View in the *bc* plane of the packing within [(*rac*)-2]I₃; Figure S8: View in the *bc* plane of the packing within [(*R,R*)-2]I₃; Figure S9: Packing of the donors and highlight of the S···S short contacts for [(*rac*)-2]I₃; Figure S10: Packing diagram for (*meso*)-2; Figure S11: Solid state structure of [(*meso*)-2]PF₆; Figure S12: Molecular structure of [(*meso*)-2]ClO₄; Figure S13: Molecular structure of [(*meso*)-2]ReO₄; Figure S14: Packing diagram for [(*meso*)-2]ReO₄; Table S1: Crystal Data and Structure Refinement for [(*rac*)-

1]₂AsF₆, [(S)-1]₂AsF₆ and [(R)-1]₂AsF₆; Table S2: C–H⋯F hydrogen bonding distances (Å) and angles in [(rac)-1]₂AsF₆; Table S3: C–H⋯F hydrogen bonding distances (Å) and angles in [(S)-1]₂AsF₆; Table S4: Crystal Data and Structure Refinement for [(S)-1]AsF₆·C₄H₈O and [(R)-1]AsF₆·C₄H₈O; Table S5: C–H⋯F hydrogen bonding distances (Å) and angles in [(S)-1]AsF₆·C₄H₈O; Table S6: C–H⋯F hydrogen bonding distances (Å) and angles in [(R)-1]AsF₆·C₄H₈O; Table S7: Crystal Data and Structure Refinement for [(rac)-1]I₃, [(S)-1]I₃ and [(R)-1]I₃; Table S8: Selected C = C and C–S internal bond lengths for [(S)-1]I₃; Table S9: Crystal Data and Structure Refinement for [(rac)-2]I₃, [(S,S)-2]I₃ and [(R,R)-2]I₃; Table S10: Selected C = C and C–S internal bond lengths for (2)I₃; Table S11: Crystal Data and Structure Refinement for (meso)-2, [(meso)-2]ClO₄, [(meso)-2]PF₆ and [(meso)-2]ReO₄; Table S12: Selected C = C and C–S internal bond lengths for (meso)-2, [(meso)-2]ClO₄, [(meso)-2]PF₆ and [(meso)-2]ReO₄.

Author Contributions: N.A. conceived and designed the experiments; N.M., A.B. and F.P. synthesized and characterized the materials; N.V. performed the chiral HPLC separation of precursor **1**; P.A.-S., E.B.L. and M.A. investigated the electron transport properties; N.A. and F.P. wrote and/or reviewed the manuscript with contributions from all authors. All authors have read and agreed to the published version of the manuscript.

Funding: This research was partially funded in France by the National Agency for Research (ANR), Project 15-CE29-0006-01 ChiraMolCo, French Ministry of Europe and Foreign Affairs through the Eiffel Program (grant to A.B.), and in Portugal by FCT under contracts UIDB/04349/2020 and LISBOA-01-0145-FEDER-029666.

Institutional Review Board Statement: Not applicable.

Acknowledgments: This work was supported in France by the CNRS and the University of Angers. Magali Allain (MOLTECH-Anjou, University of Angers) is warmly thanked for help with the single crystal X-ray structure refinement. The collaboration between the Portuguese and French team members was also supported by a FCT–French Ministry of Foreign Affairs bilateral action FCT/PHC-PESSOA 2020-21 (Project 44647UB).

Conflicts of Interest: The authors declare no conflict of interest.

References

1. Avarvari, N.; Wallis, J.D. Strategies Towards Chiral Molecular Conductors. *J. Mater. Chem.* **2009**, *19*, 4061–4076. [[CrossRef](#)]
2. Pop, F.; Zigon, N.; Avarvari, N. Main-Group-Based Electro- and Photoactive Chiral Materials. *Chem. Rev.* **2019**, *119*, 8435–8478. [[CrossRef](#)]
3. Mroweh, N.; Auban-Senzier, P.; Vanthuyne, N.; Canadell, E.; Avarvari, N. Chiral EDT-TTF precursors with one stereogenic centre: Substituent size modulation of the conducting properties in the (R-EDT-TTF)₂PF₆ (R = Me or Et) series. *J. Mater. Chem. C* **2019**, *7*, 12664–12673. [[CrossRef](#)]
4. Mroweh, N.; Auban-Senzier, P.; Vanthuyne, N.; Lopes, E.B.; Almeida, M.; Canadell, E.; Avarvari, N. Chiral Conducting Me-EDT-TTF and Et-EDT-TTF Based Radical Cation Salts with the Perchlorate Anion. *Crystals* **2020**, *10*, 1069. [[CrossRef](#)]
5. Pop, F.; Auban-Senzier, P.; Frackowiak, A.; Ptaszyński, K.; Olejniczak, I.; Wallis, J.D.; Canadell, E.; Avarvari, N. Chirality Driven Metallic versus Semiconducting Behavior in a Complete Series of Radical Cation Salts Based on Dimethyl-Ethylenedithio-Tetrathiafulvalene (DM-EDT-TTF). *J. Am. Chem. Soc.* **2013**, *135*, 17176–17186. [[CrossRef](#)] [[PubMed](#)]
6. Rikken, G.L.J.A.; Fölling, J.; Wyder, P. Electrical Magneto-chiral Anisotropy. *Phys. Rev. Lett.* **2001**, *87*, 236602. [[CrossRef](#)] [[PubMed](#)]
7. Krstić, V.; Roth, S.; Burghard, M.; Kern, K.; Rikken, G.L.J.A. Magneto-Chiral Anisotropy in Charge Transport Through Single-Walled Carbon Nanotubes. *J. Chem. Phys.* **2002**, *117*, 11315–11319. [[CrossRef](#)]
8. Pop, F.; Auban-Senzier, P.; Canadell, E.; Rikken, G.L.J.A.; Avarvari, N. Electrical magneto-chiral anisotropy in a bulk chiral molecular conductor. *Nat. Commun.* **2014**, *5*, 3757. [[CrossRef](#)] [[PubMed](#)]
9. Pop, F.; Auban-Senzier, P.; Canadell, E.; Avarvari, N. Anion size control of the packing in the metallic versus semiconducting chiral radical cation salts (DM-EDT-TTF)₂XF₆ (X = P, As, Sb). *Chem. Commun.* **2016**, *52*, 12438–12441. [[CrossRef](#)]
10. Mroweh, N.; Mézière, C.; Allain, M.; Auban-Senzier, P.; Canadell, E.; Avarvari, N. Conservation of structural arrangements and 3:1 stoichiometry in a series of crystalline conductors of TMTTF, TMTSF, BEDT-TTF, and chiral DM-EDT-TTF with the oxo-bis[pentafluorotantalate(V)] dianion. *Chem. Sci.* **2020**, *11*, 10078–10091. [[CrossRef](#)]
11. Yagubskii, E.B.; Shchegolev, I.F.; Laukhin, V.N.; Kononovich, P.A.; Kartsovnik, M.V.; Zvarykina, A.V.; Buravov, L.I. Normal-pressure superconductivity in an organic metal (BEDT-TTF)₂I₃ [bis(ethylene dithiolo) tetrathiofulvalene triiodide]. *JETP Lett.* **1984**, *39*, 12–16.
12. Crabtree, G.W.; Carlson, K.D.; Hall, L.N.; Copps, P.T.; Wang, H.H.; Emge, T.J.; Beno, M.A.; Williams, J.M. Superconductivity at ambient pressure in di[bis(ethylenedithio)tetrathiafulvalene] triiodide, (BEDT-TTF)₂I₃. *Phys. Rev. B* **1984**, *30*, 2958–2960. [[CrossRef](#)]

13. Tokumoto, M.; Murata, K.; Bando, H.; Anzai, H.; Saito, G.; Kajimura, K.; Ishiguro, T. Ambient-pressure superconductivity at 8 K in the organic conductor β -(BEDT-TTF)₂I₃. *Solid State Commun.* **1985**, *54*, 1031–1034. [[CrossRef](#)]
14. Wallis, J.D.; Karrer, A.; Dunitz, J.D. Chiral metals? A chiral substrate for organic conductors and superconductors. *Helv. Chim. Acta* **1986**, *69*, 69–70. [[CrossRef](#)]
15. Pop, F.; Laroussi, S.; Cauchy, T.; Gómez-García, C.J.; Wallis, J.D.; Avarvari, N. Tetramethyl-Bis(ethylenedithio)-Tetrathiafulvalene (TM-BEDT-TTF) Revisited: Crystal Structures, Chiroptical Properties, Theoretical Calculations, and a Complete Series of Conducting Radical Cation Salts. *Chirality* **2013**, *25*, 466–474. [[CrossRef](#)] [[PubMed](#)]
16. Karrer, A.; Wallis, J.D.; Dunitz, J.D.; Hilti, B.; Mayer, C.W.; Bürkle, M.; Pfeiffer, J. Structures and Electrical Properties of Some New Organic Conductors Derived from the Donor Molecule TMET (*S,S,S,S*-Bis(dimethylethylenedithio) tetrathiafulvalene). *Helv. Chim. Acta* **1987**, *70*, 942–953. [[CrossRef](#)]
17. Galán-Mascarós, J.R.; Coronado, E.; Goddard, P.A.; Singleton, J.; Coldea, A.I.; Wallis, J.D.; Coles, S.J.; Alberola, A. A Chiral Ferromagnetic Molecular Metal. *J. Am. Chem. Soc.* **2010**, *132*, 9271–9273. [[CrossRef](#)] [[PubMed](#)]
18. Pop, F.; Mézière, C.; Allain, M.; Auban-Senzier, P.; Tajima, N.; Hirobe, D.; Yamamoto, H.M.; Canadell, E.; Avarvari, N. Unusual stoichiometry, band structure and band filling in conducting enantiopure radical cation salts of TM-BEDT-TTF showing helical packing of the donors. *J. Mater. Chem. C* **2021**, *9*. [[CrossRef](#)]
19. Matsumiya, S.; Izuoka, A.; Sugawara, T.; Taruishi, T.; Kawada, Y. Effect of Methyl Substitution on Conformation and Molecular Arrangement of BEDT-TTF Derivatives in the Crystalline Environment. *Bull. Chem. Soc. Jpn.* **1993**, *66*, 513–522. [[CrossRef](#)]
20. Mroweh, N.; Mézière, C.; Pop, F.; Auban-Senzier, P.; Alemany, P.; Canadell, E.; Avarvari, N. In Search of Chiral Molecular Superconductors: κ -[(*S,S*)-DM-BEDT-TTF]₂ClO₄ Revisited. *Adv. Mater.* **2020**, *32*, 2002811. [[CrossRef](#)]
21. Matsumiya, S.; Izuoka, A.; Sugawara, T.; Taruishi, T.; Kawada, Y.; Tokumoto, M. Crystal Structure and Conductivity of Chiral Radical Ion Salts (Me₂ET)₂X. *Bull. Chem. Soc. Jpn.* **1993**, *66*, 1949–1954. [[CrossRef](#)]
22. Kimura, S.; Maejima, T.; Suzuki, H.; Chiba, R.; Mori, H.; Kawamoto, T.; Mori, T.; Moriyama, H.; Nishio, Y.; Kajita, K. A new organic superconductor β -(*meso*-DMBEDT-TTF)₂PF₆. *Chem. Commun.* **2004**, *21*, 2454–2455. [[CrossRef](#)] [[PubMed](#)]
23. Kimura, S.; Suzuki, H.; Maejima, T.; Mori, H.; Yamaura, J.-I.; Kakiuchi, T.; Sawa, H.; Moriyama, H. Checkerboard-Type Charge-Ordered State of a Pressure-Induced Superconductor, β -(*meso*-DMBEDT-TTF)₂PF₆. *J. Am. Chem. Soc.* **2006**, *128*, 1456–1457. [[CrossRef](#)] [[PubMed](#)]
24. Hountas, A.; Terzis, A.; Papavassiliou, G.C.; Hilti, B.; Pfeiffer, J. Structures of the Conducting Salts of Ethylenedithiotetrathiafulvalene (EDTTTF) and Methylenedithiotetrathiafulvalene (MDTTTF): (EDTTTF)₃ and (MDTTTF)₃. *Acta Cryst. C* **1990**, *C46*, 220–223. [[CrossRef](#)]
25. Cauchy, T.; Pop, F.; Cuny, J.; Avarvari, N. Conformational Study and Chiroptical Properties of Chiral Dimethyl-Ethylenedithio-Tetrathiafulvalene (DM-EDT-TTF). *Chimia* **2018**, *72*, 389–393. [[CrossRef](#)]
26. Abhervé, A.; Mroweh, N.; Cauchy, T.; Pop, F.; Cui, H.; Kato, R.; Vanthuyne, N.; Alemany, P.; Canadell, E.; Avarvari, N. Conducting chiral nickel(II) bis(dithiolene) complexes: Structural and electron transport modulation with the charge and the number of stereogenic centres. *J. Mater. Chem. C* **2021**, *9*, 4119–4140. [[CrossRef](#)]
27. Atzori, M.; Pop, F.; Auban-Senzier, P.; Clérac, R.; Canadell, E.; Mercuri, M.L.; Avarvari, N. Complete Series of Chiral Paramagnetic Molecular Conductors Based on Tetramethyl-bis(ethylenedithio)-tetrathiafulvalene (TM-BEDT-TTF) and Chloranilate-Bridged Heterobimetallic Honeycomb Layers. *Inorg. Chem.* **2015**, *54*, 3643–3653. [[CrossRef](#)]
28. Coronado, E.; Galán-Mascarós, J.R.; Gómez-García, C.; Laukhin, V. Coexistence of ferromagnetism and metallic conductivity in a molecule-based layered compound. *Nature* **2000**, *408*, 447–449. [[CrossRef](#)] [[PubMed](#)]
29. Rashid, S.; Turner, S.S.; Day, P.; Howard, J.A.K.; Guionneau, P.; McInnes, E.J.L.; Mabbs, F.E.; Clark, R.J.H.; Firth, S.; Biggs, T. New Superconducting Charge-Transfer Salts (BEDT-TTF)₄[A·M(C₂O₄)₃]·C₆H₅NO₂ (A = H₃O or NH₄, M = Cr or Fe, BEDT-TTF = Bis(Ethylenedithio)Tetrathiafulvalene). *J. Mater. Chem.* **2001**, *11*, 2095–2101. [[CrossRef](#)]
30. Uji, S.; Shinagawa, H.; Terashima, T.; Yakabe, T.; Terai, Y.; Tokumoto, M.; Kobayashi, A.; Tanaka, H.; Kobayashi, H. Magnetic-Field-Induced Superconductivity in a Two-Dimensional Organic Conductor. *Nature* **2001**, *410*, 908–910. [[CrossRef](#)] [[PubMed](#)]
31. Kurmoo, M.; Graham, A.W.; Day, P.; Coles, S.J.; Hursthouse, M.B.; Caulfield, J.L.; Singleton, J.; Pratt, F.L.; Hayes, W.; Ducasse, L.; et al. Superconducting and Semiconducting Magnetic Charge Transfer Salts: (BEDT-TTF)₄AFe(C₂O₄)₃·C₆H₅CN (A = H₂O, K, NH₄). *J. Am. Chem. Soc.* **1995**, *117*, 12209–12217. [[CrossRef](#)]
32. Martin, L.; Lopez, J.R.; Akutsu, H.; Nakazawa, Y.; Imajo, S. Bulk Kosterlitz–Thouless Type Molecular Superconductor β'' -(BEDTTTF)₂[(H₂O)(NH₄)₂Cr(C₂O₄)₃]₁₈-crown-6. *Inorg. Chem.* **2017**, *56*, 14045–14052. [[CrossRef](#)]
33. Chaikin, P.M.; Kwak, J.F. Apparatus for thermopower measurements on organic conductors. *Rev. Sci. Instrum.* **1975**, *46*, 218–220. [[CrossRef](#)]
34. Almeida, M.; Alcácer, L.; Oostra, S. Anisotropy of thermopower in *N*-methyl-*N*-ethylmorpholinium bistetracyanoquinodimethane, MEM(TCNQ)₂, in the region of the high-temperature phase transitions. *Phys. Rev. B* **1984**, *30*, 2839–2844. [[CrossRef](#)]
35. Lopes, E.B. *INETI-Sacavém*; Internal Report; INETI Press: Sacavém, Portugal, 1991.
36. Huebener, R.P. Thermoelectric Power of Lattice Vacancies in Gold. *Phys. Rev.* **1964**, *135*, A1281–A1291. [[CrossRef](#)]